International Journal of Nanomedicine

Dovepress
open access to scientific and medical research

Open Access Full Text Article

ORIGINAL RESEARCH

Ultrasound -Induced Thermal Effect Enhances the Efficacy of Chemotherapy and Immunotherapy in Tumor Treatment

Yuting Xiang[1,2,*], Li Tang[1,*], Hua Pang[3], Han Xu[1,2], Yiman He[1,2], Yuyue Feng[3], Linjun Ju[3], Liang Zhang[1], Dong Wang[1]

[1]Department of Ultrasound, The First Affiliated Hospital of Chongqing Medical University, Chongqing, People's Republic of China; [2]Chongqing Key Laboratory of Ultrasound Molecular Imaging, Chongqing Medical University, Chongqing, People's Republic of China; [3]Department of Nuclear Medicine, The First Affiliated Hospital of Chongqing Medical University, Chongqing, People's Republic of China

*These authors contributed equally to this work

Correspondence: Liang Zhang; Dong Wang, Department of Ultrasound, The First Affiliated Hospital of Chongqing Medical University, 1 Youyi Road, Yuzhong District, Chongqing, 400042, People's Republic of China, Email zhangliang338@cqmu.edu.cn; wang57554@163.com

Background: The inadequate perfusion, frequently resulting from abnormal vascular configuration, gives rise to tumor hypoxia. The presence of this condition hinders the effective delivery of therapeutic drugs and the infiltration of immune cells into the tumor, thereby compromising the efficacy of treatments against tumors. The objective of this study is to exploit the thermal effect of ultrasound (US) in order to induce localized temperature elevation within the tumor, thereby facilitating vasodilation, augmenting drug delivery, and enhancing immune cell infiltration.

Methods: The selection of US parameters was based on intratumor temperature elevation and their impact on cell viability. Vasodilation and hypoxia improvement were investigated using enzyme-linked immunosorbent assay (ELISA) and immunofluorescence examination. The distribution and accumulation of commercial pegylated liposomal doxorubicin (PLD) and PD-L1 antibody (anti-PD-L1) in the tumor were analyzed through frozen section analysis, ELISA, and in vivo fluorescence imaging. The evaluation of tumor immune microenvironment was conducted using flow cytometry (FCM). The efficacy of US-enhanced chemotherapy in combination with immunotherapy was investigated by monitoring tumor growth and survival rate after various treatments.

Results: The US irradiation condition of 0.8 W/cm^2 for 10 min effectively elevated the tumor temperature to approximately 40 °C without causing any cellular or tissue damage, and sufficiently induced vasodilation, thereby enhancing the distribution and delivery of PLD and anti-PD-L1 in US-treated tumors. Moreover, it effectively mitigated tumor hypoxia while significantly increasing M1-phenotype tumor-associated macrophages (TAMs) and CD8+ T cells, as well as decreasing M2-phenotype TAMs. By incorporating US irradiation, the therapeutic efficacy of PLD and anti-PD-L1 was substantially boosted, leading to effective suppression of tumor growth and prolonged survival in mice.

Conclusion: The application of US (0.8 W/cm^2 for 10 min) can effectively induce vasodilation and enhance the delivery of PLD and anti-PD-L1 into tumors, thereby reshaping the immunosuppressive tumor microenvironment and optimizing therapeutic outcomes.

Keywords: ultrasound, thermal effect, vasodilatation, drug delivery, tumor microenvironment

Introduction

The concurrent utilization of chemotherapy and immunotherapy represents a prevailing approach in the field of cancer treatment.[1,2] Optimizing the concentration of chemotherapeutic drugs in tumor tissues is crucial for enhancing their therapeutic efficacy. Tumor immunotherapy, particularly immune checkpoint blockade, reshapes the tumor microenvironment and strengthens the body's anti-tumor immune response, thereby contributing to more effective tumor eradication.[3,4] Specifically, immune checkpoint blockade, such as the inhibition of programmed cell death protein 1 (PD-1)/programmed cell death ligand 1 (PD-L1) interaction, has exhibited remarkable efficacy in the treatment of diverse

Received: 25 March 2024
Accepted: 11 June 2024
Published: 3 July 2024

malignancies.[5–7] However, the therapeutic efficacy of these treatments is often hindered by limited accumulation of PD-L1 antibody (anti-PD-L1) and inadequate infiltration of T cells, particularly $CD8^+$ T cells, within the tumor microenvironment.[8,9] The significance of optimizing the intratumoral concentration of therapeutic drugs, including anti-PD-L1 and pegylated liposomal doxorubicin (PLD), as well as augmenting $CD8^+$ T cell infiltration, cannot be overstated in order to maximize the effectiveness of treatment.

The limited presence of drugs and immune cells in tumors during their progression is partially attributed to the tumor's aberrant vascular system within the tumor.[10] The blood vessels in tumors, unlike their normal counterparts, frequently exhibit disorganization characterized by irregular branching patterns and varying thicknesses. The disorganized structure gives rise to physiological challenges, such as compromised perfusion and uneven blood flow distribution, which hinder the diffusion of antitumor drugs and impede the infiltration of $CD8^+$ T cells.[11,12] Additionally, the aberrant vascular system results in a hypoxic tumor microenvironment, thereby promoting resistance to chemotherapy and exacerbating immunosuppression. The concept of normalizing tumor blood vessels to enhance drug and immune cell penetration was initially proposed by Rakesh K. Jain in 2001.[13] This innovative approach, which utilizes anti-angiogenic drugs to transiently normalize tumor blood vessels, has demonstrated potential in augmenting the therapeutic efficacy of anticancer medications. The well-established vasodilatory properties of nitric oxide (NO) have led to the utilization of 1.3-bis-(2,4,6-trimethylphenyl)imidazolylidene nitric oxide (IMesNO) as an NO donor in studies, resulting in enhanced vasodilation and increased uptake of doxorubicin (DOX).[14] The prolonged use of these drugs, despite their initial benefits, may potentially result in drug resistance and exacerbation of tumor hypoxia, posing a significant clinical challenge.[15,16] Currently, numerous studies have employed diverse nanocarriers to enhance the drug penetration and concentration in tumors, including nanoparticles, micelles, liposomes, and even novel drug delivery carriers developed on this foundation such as deformable nanocarriers and self-nanoemulsifying drug delivery system.[17–20] The various delivery methods, while offering advantages such as prolonged drug circulation, precise drug release, and enhanced drug bioavailability, often entail the introduction of additional materials into the body which may lead to certain toxic side effects.[21,22]

The application of hyperthermia as a cancer treatment modality is highly esteemed due to its non-toxic and safety, thus establishing itself as an green therapeutic method.[23] The blood flow is believed to facilitate the dissipation of heat from the surrounding tissues of the blood vessels, thereby impeding the attainment of the required level of heating in hyperthermia.[24] However, tumor tissues exhibit aberrant blood vessels and a sluggish blood flow rate, which attenuates the local tissue's capacity for heat dissipation and enables effective heat accumulation during hyperthermia.[24] Hyperthermia is typically categorized into hyperthermia ablation and mild-hyperthermia therapy.[25,26] Commonly employed methods of hyperthermia ablation include microwave, radiofrequency, and high-intensity focused ultrasound (HIFU) thermal ablation techniques.[2] While hyperthermia ablation can directly eradicate the tumor, it also disrupts the internal blood vessels of the tumor, thereby impacting the subsequent penetration of therapeutic drugs into the tumor. Moreover, sharply elevated temperatures can cause adjacent healthy tissues to experience a rise in temperature and impair normal cellular function. Mild-hyperthermia therapy is a therapeutic approach that utilizes mild heat to enhance the permeability of tumor blood vessels and expand the pores of tumor microvessels, thereby facilitating improved penetration of therapeutic drugs and minimizing damage to surrounding normal tissues.[27–30] Clinical evidence has consistently demonstrated that combining hyperthermia with chemotherapy effectively enhances local tumor control rates and prolongs patient survival.[31] Xia et al synthesized photo-responsive gold nanoparticles (AuNPs), which exhibited laser-induced accumulation towards the tumor and generated photothermal effects at the tumor site.[32] In vivo experiments conducted on 4T1 tumor-bearing mice demonstrated that laser-induced thermal effects significantly promoted local blood vessel expansion within the tumor area, thereby effectively enhancing the enrichment of chemotherapeutic drugs in the tumor tissue. The tissue penetration depth of lasers, however, is limited, thereby resulting in suboptimal therapeutic efficacy.[33] US, on the other hand, offers a non-invasive and non-radiative approach with high penetration capabilities and precise tunability for active targeted drug delivery, making it widely employed in tumor treatment research.[34,35] In addition to its mechanical effects, US also exhibits a significant thermal effect. Compared to other hyperthermia methods, the exceptional tissue penetration capability of US enables effective conversion of sound

energy into heat energy at deep tumor sites.[34] Therefore, we anticipate utilizing the thermal effects of US to enhance vasodilation, facilitating improved delivery of drugs, oxygen, and $CD8^+$ T cells to tumor tissues.

In this study, US is employed to elevate the temperature in the tumor region, which is expected to dilate tumor blood vessels, alleviating intratumoral hypoxia, and reprogramming immunosuppressive tumor microenvironment (Scheme 1). US irradiation is anticipated to enhance the accumulation of commercial PLD, anti-PD-L1, and $CD8^+$ T cells in the tumor, potentially improving the efficacy of tumor chemotherapy and immunotherapy.

Materials and Methods

Materials and Reagents

PLD was obtained from Zhangjiang Bio-Pharmaceutical Co., Ltd. (Shanghai, China). Anti-PD-L1 was obtained from BioXCell (Lebanon, NH, USA). Cell counting kit-8 (CCK-8) assay was obtained from MedChemExpress (Shanghai, China). 2-(4-amidinophenyl)-6-indolecarbamidinedihydrochloride (DAPI) was obtained from Beyotime Technology (Shanghai, China). APC-conjugated anti-mouse CD3, FITC-conjugated anti-mouse CD4, PE-conjugated anti-mouse CD8a, PerCP-CY5.5-conjugated anti-mouse CD11b, PE-conjugated anti-mouse CD86, APC-conjugated anti-mouse

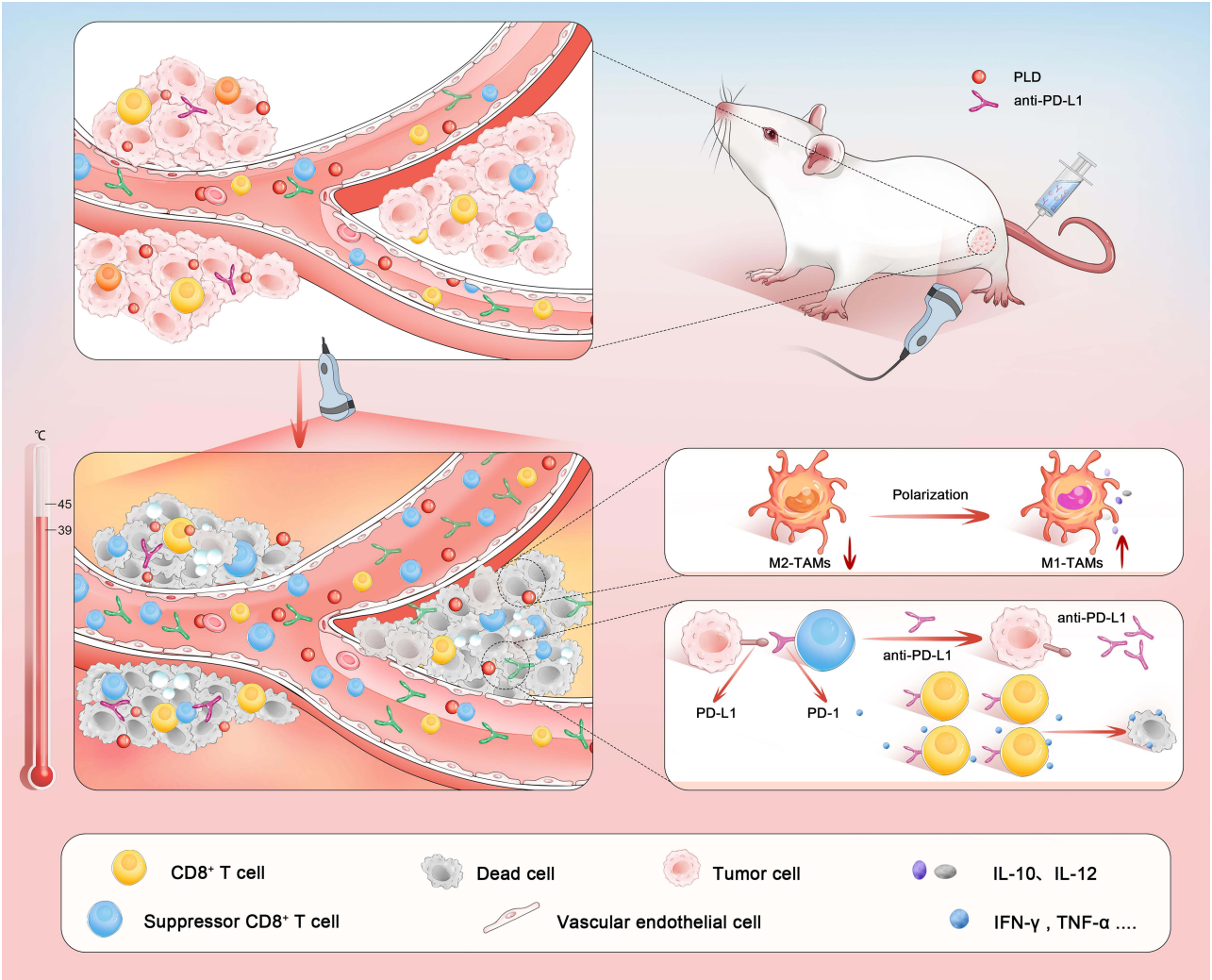

Scheme 1 A scheme illustrating a protocol for enhancing the effectiveness of chemotherapy and immunotherapy through the thermal effect derived from US. The incorporation of US irradiation can induce vasodilation, effectively facilitating the delivery of PLD, anti-PD-L1, and $CD8^+$ T cells to the tumor interior. This process alleviates hypoxia, reduces the population of M2-TAMs while increasing the proportion of M1-TAMs. Consequently, it reprograms the immunosuppressive tumor microenvironment and enhances therapeutic efficacy.

CD206, FITC-conjugated anti-mouse F4/80 were purchased from eBioscience (CA, USA). The Fix & Perm Kits was purchased from Lianke Bio (Hangzhou, China). Cyanine 5.5 NHS ester (Cy5.5) was purchased from Xi'an Ruixi Biological Technology Co., Ltd. (Xi'an, China). Interleukin-10 (IL-10), IL-12, tumor necrosis factor-α (TNF-α), interferon-γ (IFN-γ), mouse granzyme B (GZMS-B), endothelial nitric oxide synthase (eNOs), NO, prostaglandin I_2 (PGI_2), prostaglandin F_2 (PGF_2), complement fragment 5a (C5a) and leukotriene C4 (LTC4), mouse PD-L1 Ab enzyme-linked immunosorbent assay (ELISA) kits were purchased from Sumeike Biological Technology Co., Ltd. (Jiangsu, China). 5(6)-Carboxyfluorescein diacetate succinimidyl ester (CFSE) was purchased from Abcam (Shanghai, China). Evans blue (EB) was obtained from Selleck (Shanghai, China).

Cell Culture and Animal Model

CT26 murine colorectal cancer cell line was purchased from Procell Life Science & Technology Co., Ltd. (Wuhan, China). CTLL-2 cells were purchased from Jinyuan biotechnology Co., Ltd. (Shanghai, China). Murine 4T1 breast cancer cell line was obtained from Zhongqiaoxinzhou Biotechnology Co., Ltd. (Shanghai, China). These cells were incubated with the recommended medium at 37 °C under 5% CO_2.

Female BALB/c mice aged 6–8 weeks were purchased from Hunan SJA Laboratory Animal Co., Ltd. (Hunan, China). The mice were housed at the Animal Experimental Center of Chongqing Medical University, where they had unrestricted access to food and water under specific conditions in accordance with the Guidelines for Ethical Review of National Standard Laboratory Animal Welfare. All in vivo experiments have been approved by the Animal Experiment Ethics Committee of Chongqing Medical University. For the tumor grafting, CT26 cells (1×10^6) in 50 μL phosphate-buffered solution (PBS) suspension was inoculated subcutaneously on the left lower back of mice, and the 4T1 cells was inoculated in situ breast. The status of tumor and mice were monitored every other day. The tumors volumes were calculated by the formula: $V = [\text{length} \times (\text{width})^2/2]$.

Cytotoxicity Assay

CCK-8 assay was conducted to assess cell viability at different US intensities. CT26 cells were seeded in 96-well plates at a density of 5×10^3 cells per well. After 24 h, the cells were treated with varying intensities of US. Post-treatment, all cells were incubated for an additional 24 h. Cell medium in each well was then replaced by 100 μL of 10% CCK-8 solution diluted in 1640 basal medium in the dark at 37°C for 40 min. The absorbance of each well was subsequently measured by a microplate reader at 560 nm.

US-Induced Vasodilation

The unilateral CT26 tumor-bearing mice were randomly allocated into two groups: a Control group and a US treatment group (0.8 W/cm^2, 10 min). To assess the vasodilatation and vascular regeneration following US treatment, mice were euthanized 24 h post-treatment. One mouse in each group was then harvested for hematoxylin and eosin (H&E) staining and CD31 immunofluorescence staining. According to the previous report,[36] three fields of H&E staining view were selected in each section to measure the diameter of blood vessels. The mean vessel diameter (MVD) was then analyzed. Furthermore, the secretion of relevant vasodilating factors in tumor tissues was assessed 24 h after completing three sessions of US treatments. Tumor tissues were collected, weighed, and then homogenized in 1 mL of saline. The tissue homogenate was centrifuged, and the resulting supernatants were analyzed using ELISA to quantify levels of eNOs, NO, PGI2, PGF2, C5a, and LTC4 levels in the tumor tissues.

Intratumor Distribution of PLD and Anti-PD-L1

The concentrations of PLD/anti-PD-L1 in tumor tissues were quantitatively assessed. Mice in both the PLD/anti-PD-L1 group and the PLD/anti-PD-L1 + US group were euthanized 24 h after receiving the respective treatments. The tumor tissues from each group were extracted, weighed, and homogenized. After centrifugation at 3000 rpm for 10 min at 4 °C, the supernatant was retained. The fluorescence intensity was measured using a microplate reader (DOX: λex = 490 nm, λem = 560 nm). The concentration of DOX in tumor tissues was calculated based on the standard curve and measured fluorescence values. The concentration of anti-PD-L1 in tumor tissues was quantified using ELISA kits.

The distribution and accumulation of PLD and anti-PD-L1 were further assessed by fluorescence microscope and in vivo fluorescence imaging, respectively. The CT26 tumor-bearing mice were randomly allocated into two groups: the anti-PD-L1/PLD group and the anti-PD-L1/PLD + US group. For PLD observation, 24 h post-treatments, the tumor tissues were collected for frozen section, and the fluorescence microscope was used to observe the distribution and accumulation of PLD. For the preparation of Cy5.5-labeled anti-PD-L1 (Cy5.5-anti-PD-L1), transfer 10 μL of an anti-PD -L1 solution (1 mg/mL) to a centrifuge tube and supplement with 990 μL of pH-adjusted water (pH value: 8.0 adjusted using bicarbonate amine). The mixture was maintained in a shaker at a temperature of 4 °C for a duration of 12 h in order to facilitate the conjugation process between Cy5.5 and anti-PD-L1. Subsequently, any remaining unreacted dyes should be removed by passing them through the G-25 column. Cy5.5-anti-PD-L1 (30 μg/per mouse) was administered intravenously in CT26 tumor-bearing mice. Following US treatments, in vivo fluorescence imaging was performed 24 h after treatment completion, along with ex vivo fluorescence imaging of excised tumor tissues. At the same time, one tumor from each group was collected for frozen section, and the distribution of Cy5.5-anti-PD-L1 was observed using a fluorescence microscope. The 4T1 tumor-bearing mice were randomly allocated into two groups: the anti-PD-L1 group and the anti-PD-L1 + US group. Cy5.5 was used to label the anti-PD-L1. Following treatments, the tumor tissue was collected for frozen section, and examined under a fluorescence microscope to observe the distribution of Cy5.5-anti-PD-L1.

T Cell Recruitment Assay

Murine T cells (CTLL-2 cells) were cultured under the above-mentioned conditions. For the cell counting, after being trypsinized and collected via centrifugation, cells were resuspended in PBS containing 1% fetal bovine serum and counted using a microscope. The CTLL-2 cells stained with CFSE dye (1 μM) and incubated for 20 min at room temperature in the dark. After washing, cells were resuspended and subsequently administered to the mice via intravenous injection (2×10^6 cells per mouse). The US group received immediate US irradiation post-injection. 30 min after treatment, the tumor tissues were excised, homogenized, digested, and filtered to obtain a single-cell suspension, followed by a red blood cell lysis. Cells were then subjected to flow cytometry (FCM) analysis to determine the content of CFSE-labeled CTLL-2 (CFSE-CTLL-2) cells. Additionally, the tumor tissues were collected for frozen section, and the fluorescence microscope was employed to observe the distribution and accumulation of CFSE-CTLL -2 cells.

The Alleviation of Tumor Hypoxia and the Polarization of Tumor-Associated Macrophages (TAMs)

The effect of US on tumor oxyhemoglobin saturation was evaluated using the Vevo LAZR Photoacoustic (PA) Imaging System (Visual Sonics Inc., Toronto, Canada) in PA Mode 24 h after US treatment. Oxygen saturation (sO_2 Avr Total) was analyzed by measuring the ratio between oxygenated hemoglobin (λ = 850 nm) and deoxygenated hemoglobin (λ = 750 nm). Post-imaging, mice were euthanized, and the tumor tissues were fixed in 4% paraformaldehyde for hypoxia-inducible factor 1 alpha (HIF-1α) immunofluorescence detection.

The effect of US on TAMs polarization was assessed by dividing CT26 tumor-bearing mice into two groups: a control group and a US-treated group. The US group received a 10-min treatment of US (0.8 W/cm^2, 1.0 MHz). The tumor tissues were homogenized and processed into single-cell suspensions on the 9th day for FCM analyses. M1 and M2-phenotype TAMs were distinguished by $CD11b^+F4/80^+CD86^+$ and $CD11b^+F4/80^+CD206^+$, respectively. ELISA kits were used to detect the levels of IL-10 and IL-12 in serum.

In vivo Treatment

The unilateral CT26 tumor-bearing mice were randomly divided into 8 groups as follows: A: Control, B: US group, C: PLD group, D: anti-PD-L1 group, E: PLD + US group, F: anti-PD-L1 + US group, G: PLD + anti-PD-L1 group, H: PLD + anti-PD-L1 + US group. The PLD (5 mg/kg) /anti-PD-L1 (30 μg/per mouse) was administered intravenously, followed by immediate US treatment (0.8 W/cm^2, 1.0 MHz, 50% duty cycle, 10 min). Tumor volume and survival were assessed

every two days. The tumor volume was calculated using the formula: V = [length × (width)^2/2]. Mice were euthanized when tumor volume reached 1000 mm^3. On the third day, one mouse was sacrificed from each group, and tumors were harvested for H&E and terminal deoxynucleotidyl transferase-mediated dUTP-biotin nick end labeling (TUNEL) staining.

Detection of CD8$^+$ T Infiltration in Tumor Tissues

The CT26 tumor-bearing mice were divided into 8 groups, as depicted above, in order to assess T-cell infiltration. On the 9th day, tumors from each group were dissected and homogenized using digestive enzymes. The cell suspensions were derived from the digested tumors, which were subsequently centrifuged. The resulting pellet were subjected to red blood cell lysis. Following lysis, the cells were incubated with anti-CD3-APC (0.325 μg/test), anti-CD4-FITC (0.0625 μg/test), and anti-CD8-PE (0.156 μg/test) antibodies at 4°C for 30 min. The samples were subsequently analyzed using FCM. The serum levels of TNF-α, IFN-γ, and GZMS-B were quantified using ELISA kits.

EB Experiment

4T1 tumor bearing mice were randomly divided into the control group and the US group. Each mouse was intravenously injected with EB (25 mg/kg), and mice in the US group were immediately subjected to US irradiation after injection. The mice were sacrificed 2 h after the treatment, and their tumors were collected and photographed. Then, the tumors were weighed and homogenized to quantify the EB contents. The fluorescence intensity of EB was measured by a microplate reader (λex = 480 nm, λem = 610 nm).

Statistical Analysis

The data measured in the experiment was statistically analyzed with GraphPad Prism software 8.0. Results were presented as mean ± standard deviation (SD). The significance of the differences was analyzed by Student's *t*-test.

Results and Discussion

US-Induced Thermal Effect and the Corresponding Vasodilation

The capacity of US-induced thermal effect to induce vasodilation was investigated. We first evaluated the cytotoxicity of various US intensities over a 10-min irradiation period on CT26 cells using a CCK-8 assay. It was found that at an intensity of 0.8 W/cm^2, the cell survival rate exceeded 90%. However, increasing the intensity to 0.9 W/cm^2 resulted in a significant decrease in cell survival rate, dropping to approximately 70% (Figure 1A). Therefore, we selected 0.8 W/cm^2 for the subsequent experiments, ensuring negligible adverse effect induced by US in subsequent studies. It has been reported that the therapeutic temperature range of 38.5–41.5 °C can be desirable to enhance tumor perfusion and alleviate hypoxia.[37] During US treatment, the intratumor temperature was measured using a needle probe thermometer. It was observed that the temperature exceeded 38.5 °C within 2 min and rose above 40 °C by the end of the treatment (Figure 1B). Considering the involvement of relevant inflammatory factors in tumor vasodilation, we postulate that the thermal effect of US may enhance tumor vasodilation by facilitating the release of these factors. To validate this hypothesis, we quantified the secretion levels of vasodilator factors eNOs, NO, PGF_2, C5a, LTC4, and PGI_2 in tumor tissues using ELISA kits. The results demonstrated a significant increase in the secretion of these factors from the US-treated group compared to the control group (Figure 1C). Additionally, histological alterations in the tumor tissue were examined. H&E staining revealed the presence of multiple vasodilatations within the tumor tissues after US irradiation (Figure 1D). The MVD treated with US also exhibited a significant increase (Figure S1). The CD31 marker, being a widely accepted indicator of angiogenesis, prompted us to perform CD31 immunofluorescence staining on tumors in order to ascertain the primary impact of US on blood vessels. The staining did not reveal any significant difference in CD31 expression between the groups (Figure 1E and 1F), suggesting that the thermal conditions generated by US primarily induced vasodilation rather than angiogenesis within the tumor tissues.

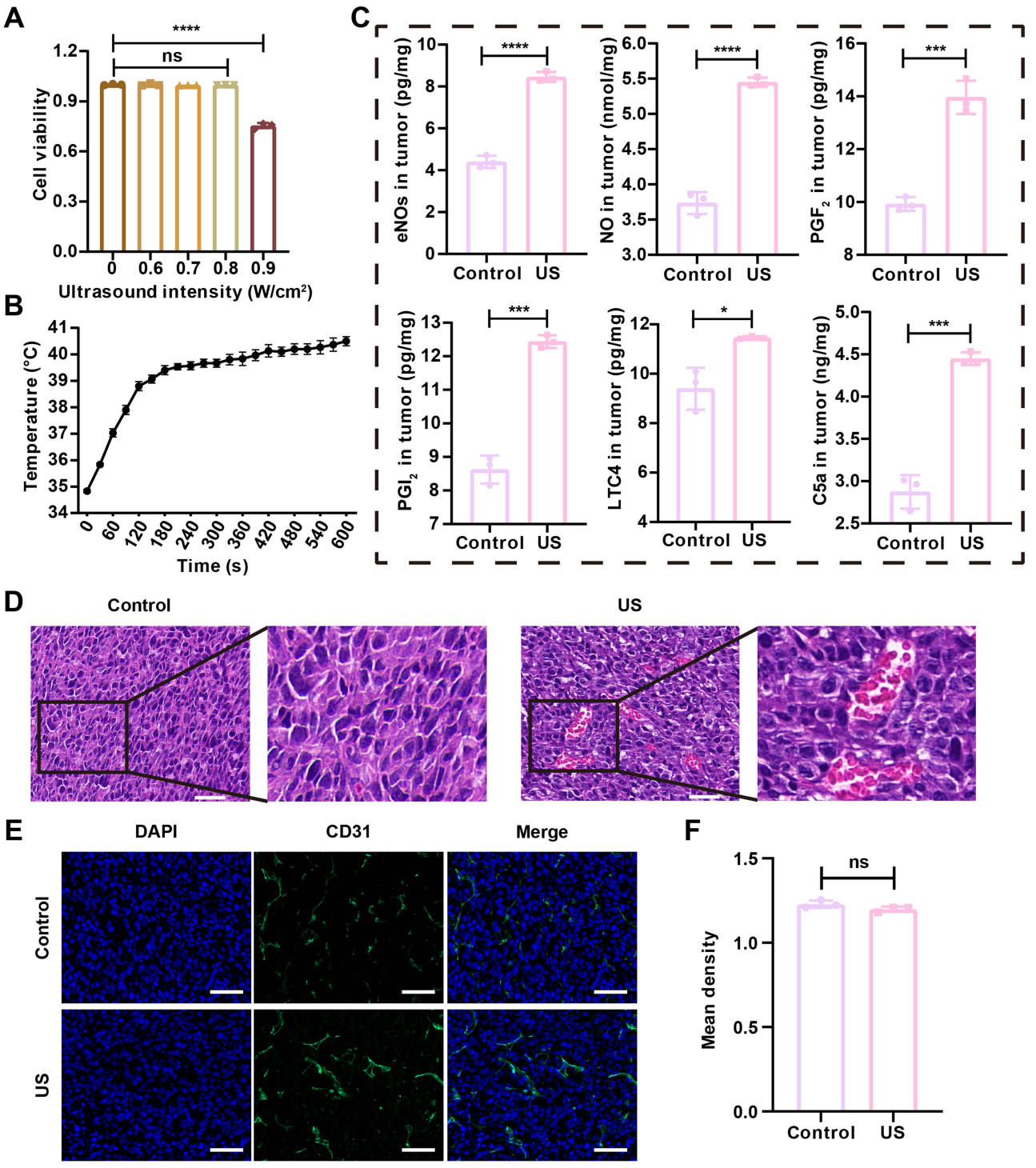

Figure 1 US thermal effect triggers vasodilation. (**A**) Cell viability of CT26 cells after exposure to various intensities of US for a duration of 10 min. (**B**) The intratumoral temperature fluctuations elicited by US. (**C**) The release of relevant vasodilating factors in tumor tissues. (**D**) H&E staining of tumor tissues after different treatments (scale bars = 20 μm). (**E-F**) CD31 immunofluorescence staining image of tumor tissues (blue: DAPI-labeled nucleus, green: CD31; scale bars = 50 μm) and corresponding quantitative analysis. Statistical significances were calculated via Student's *t* test, ns: p>0.05, *p<0.05, ***p<0.001, ****p<0.0001.

US Irradiation Promotes Intratumor Distribution of PLD, Anti-PD-L1, and T Cells

The abnormal structure of tumor blood vessels could hinder the effective delivery of immune cells and therapeutic drugs, thereby affecting the efficacy of tumor treatment.[38–40] The aforementioned experiments have confirmed that the US thermal effect could effectively dilate the blood vessels inside the tumor. It is expected that this vascular dilation can

promote the accumulation of PLD and anti-PD-L1 in tumor tissues and the infiltration of T lymphocytes. Firstly, we evaluated the intratumoral distribution of therapeutic drugs. After intravenous administration, tumors were subjected to immediate US (0.8 W/cm^2 for 10 min) exposure. The mice were sacrificed at 24 h after treatment, and frozen sections of the tumor tissues were prepared for microscopic examination. The analysis demonstrated a significantly elevated fluorescence intensity in the PLD + US group compared to the PLD-only group (Figure 2A). The drug content in tumors was quantified by homogenizing and centrifuging the tissue, followed by measuring the drug's fluorescence intensity in the supernatant using a microplate reader. The concentration of DOX was then calculated based on the standard curve correlating concentration and fluorescence intensity. The findings confirmed the elevated concentrations of PLD in US-treated tumors (Figure 2B).

Similarly, the concentration of anti-PD-L1 in tumor tissue, as measured by the mouse PD-L1 Ab ELISA kit, exhibited a significantly higher level in the group treated with US (Figure 2C). The anti-PD-L1 + US group demonstrated a significantly higher level of therapeutic drug accumulation within the tumor tissue compared to the group treated with anti-PD-L1 alone (Figure 2D, 2E and 2F), indicating that US has the potential to enhance drug accumulation in tumor tissue. Furthermore, in frozen sections of tumor tissue, we observed a significantly greater distribution of drug fluorescence in the anti-PD-L1 + US group compared to the anti-PD-L1 group, indicating that US has the potential to enhance drug accumulation within tumor tissue (Figure 2G).

Similarly, the concentration of anti-PD-L1 in tumor tissue, as measured by the mouse PD-L1 Ab ELISA kit, exhibited a significantly higher level in the group treated with US (Figure 2C). The anti-PD-L1 + US group demonstrated a significantly higher level of therapeutic drug accumulation within the tumor tissue compared to the group treated with anti-PD-L1 alone (Figure 2D, 2E and 2F), indicating that US has the potential to enhance drug accumulation in tumor tissue. Furthermore, in frozen sections of tumor tissue, we observed a significantly greater distribution of drug fluorescence in the anti-PD-L1 + US group compared to the anti-PD-L1 group, indicating that US has the potential to enhance drug accumulation within tumor tissue (Figure 2G).

The infiltration of CD8$^+$ T cells plays a pivotal role in enhancing the response to anti-PD-L1.[41,42] We postulated that US-induced vasodilation could effectively enhance the infiltration of CD8$^+$ T cells into tumor tissue. CTLL-2 cells were labeled with CFSE in vitro and subsequently reintroduced into the mice intravenously. The CFSE-CTLL-2 cell population in the tumor tissue was quantified using FCM. The FCM results revealed a 2.4-fold increase in CFSE-CTLL-2 cells in the tumor tissues of US-treated mice compared to the control group (Figure 2H and 2I). Similarly, the immunofluorescence results of tumors revealed a significantly larger distribution area of CFSE-CTLL-2 cells in the US-treated group (Figure 2J). The collective findings indicate that the thermal effects induced by US significantly enhance the intratumoral recruitment of T cells.

To further elucidate the role of US-induced thermal effects in facilitating drug delivery, we established 4T1 tumor models. After conducting an EB enrichment experiment, it was observed that tumor tissues exhibited a higher intensity of blue color following US irradiation (Figure S2A). Through quantitative analysis of the fluorescence intensity within tumors, we discovered a significant increase in the concentration of EB in the US group (Figure S2B). Subsequently, the distribution of anti-PD-L1 was investigated. The results from immunofluorescence experiments revealed that Cy5.5-anti-PD-L1 exhibited a broader fluorescence distribution and higher intensity in tumor tissue in the anti-PD-L1 + US group (Figure S2C). This observation suggests a significant increase in PD-L1 concentration within the tumor following US irradiation. Finally, immunofluorescence slices demonstrated enhanced infiltration of T cells into tumor tissue in the US group, as indicated by an augmented presence of CFSE green fluorescence with greater intensity (Figure S2D). The findings suggest that utilizing ultrasonic thermal effects to enhance drug delivery holds great promise as a viable strategy for various types of tumors.

US Irradiation Enables Tumor Hypoxia Attenuation

Given that hypoxia is a hallmark of solid tumors, which not only contributes to chemotherapy resistance but also limited the efficacy of immunotherapy.[43–46] The aforementioned experiments have demonstrated that US irradiation can effectively induce vasodilation, thereby enhancing tumor oxygen delivery and subsequently alleviating hypoxia. Consequently, the efficacy of US irradiation in mitigating tumor hypoxia was evaluated. The hypoxic environment of

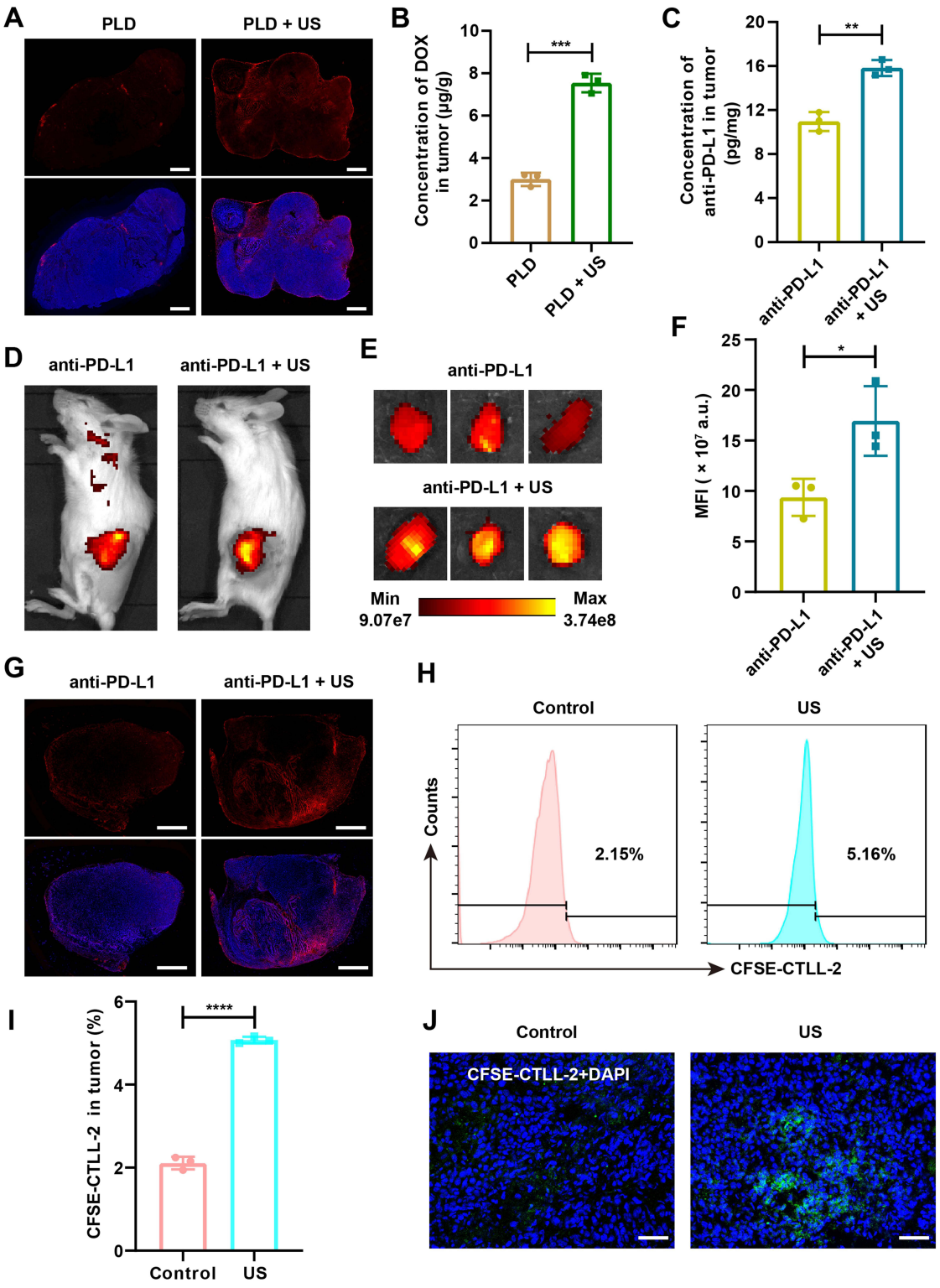

Figure 2 US irradiation promotes intratumor distribution of PLD, anti-PD-L1, and T cells. (**A**) Microscopic observation of intertumoral distribution of DOX following PLD and PLD + US treatments (blue: DAPI-labeled nucleus, red: PLD; scale bars = 2000 μm). (**B**) Quantification of DOX concentration in tumor tissue. (**C**) Quantitative assessment of the concentration of anti-PD-L1 in tumor tissues. (**D**) Representative in vivo fluorescence images of mice administered with Cy5.5-anti-PD-L1 with or without US irradiation. (**E-F**) Ex vitro fluorescence imaging and quantitative analysis of fluorescence intensity in CT26 mouse tumors following various treatments (n = 3). (**G**) Microscopic observation of intertumoral distribution of Cy5.5-anti-PD-L1 with or without US irradiation (blue: DAPI-labeled nucleus, red: Cy5.5-anti-PD-L1; scale bars = 2000 μm). (**H-I**) Representative FCM images and quantitative analysis of CFSE-CTLL-2 cells in tumor tissues with or without US irradiation (n = 3). (**J**) immunofluorescence images of tumor tissue following reinfusion of CFSE-CTLL-2 cells, with or without subsequent US treatment (blue: DAPI-labeled nucleus, green: CFSE; scale bars = 100 μm). Statistical significances were calculated via Student's *t* test, ns: p>0.05, **p<0.01, ***p<0.001, ****p<0.0001.

the tumor typically activates HIF-1α, a key regulator this condition.[47–49] The level of HIF-1α in tumor was assessed by euthanizing mice 24 h after treatment and collecting tumor samples for HIF-1α immunofluorescence staining. The findings demonstrated a significant decrease in the expression of HIF-1α within the tumor tissue of the group subjected to US treatment (Figure 3A). This implies that US irradiation effectively alleviated tumor hypoxia, potentially augmenting the therapeutic efficacy of drugs. Additionally, in order to further assess the alleviation of intratumoral hypoxia, the levels of intratumoral oxygenated hemoglobin in CT26 tumor-bearing mice from both groups were evaluated using a PA imaging system before and 24 h after treatment. The US treatment led to

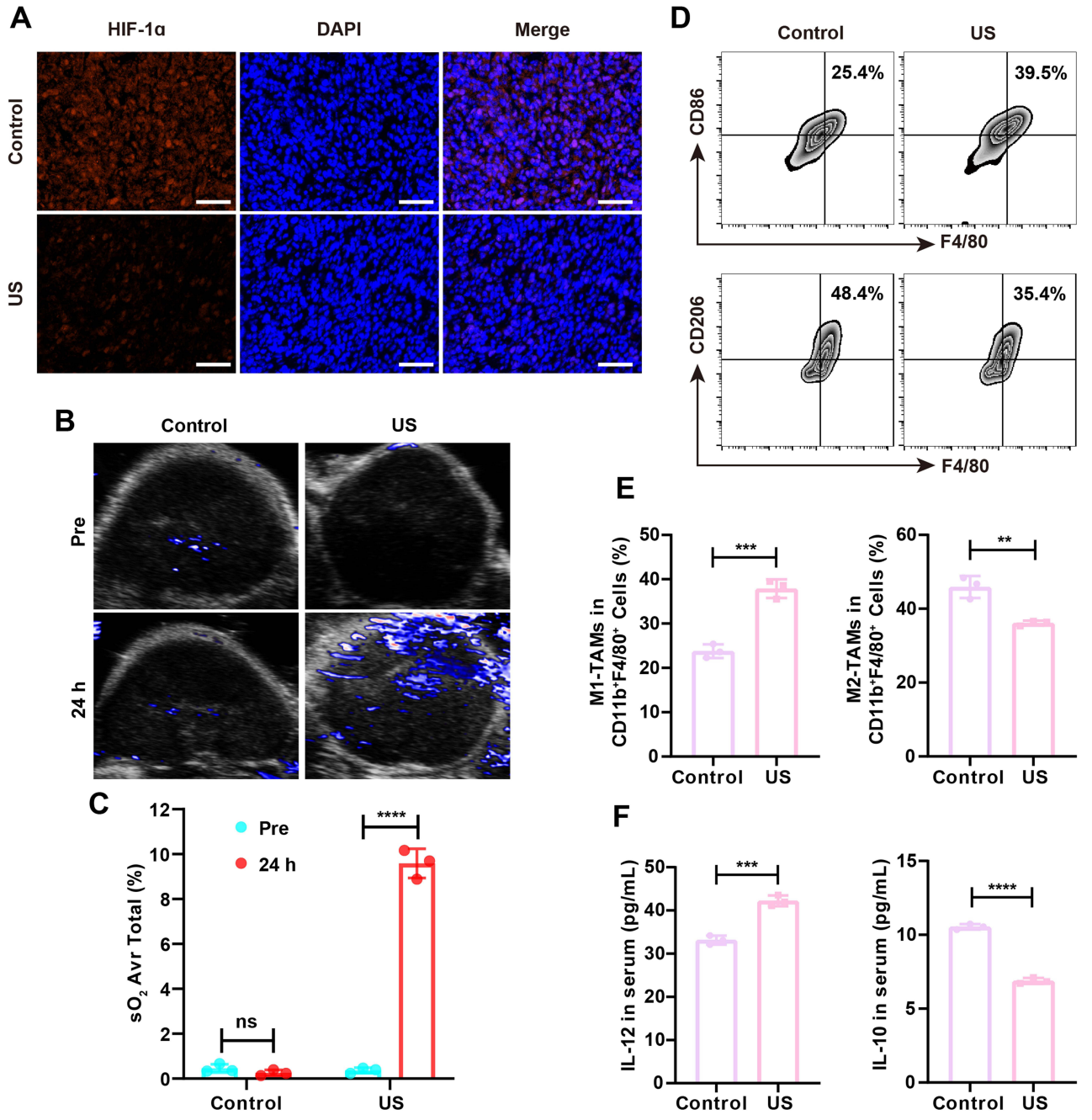

Figure 3 The alleviation of tumor hypoxia and the polarization of TAMs following US treatment. (**A**) HIF-1α immunofluorescence staining of the tumors after different treatments (blue: DAPI-labeled nucleus, red: HIF-1α; scale bars = 50 μm). (**B-C**) Representative PA images of tumors after different treatments in oxyhemoglobin mode and the corresponding quantitative analysis of oxyhemoglobin saturation within tumors (n = 3). (**D-E**) Representative FCM images and corresponding quantitative analysis of different phenotypes of TAMs in $CD11b^+F4/80^+$ cells after different treatments (M2-TAMs gated on $CD206^+$, M1-TAMs gated on $CD86^+$) (n = 3). (**F**) Cytokine levels of IL-12 and IL-10 in serum post various treatments (n = 3). Statistical significances were calculated via Student's *t* test, ns: p>0.05, **p<0.01, ***p<0.001, ****p<0.0001.

a significant increase in signals of oxygenated hemoglobin, indicating an enhanced oxygen content within the tumors (Figure 3B and 3C).

Under the induction of tumor hypoxia, the majority of TAMs exhibit an M2 phenotype, resulting in upregulated expression of inhibitory molecules that suppress anti-tumor immune response.[50,51] The alleviation of hypoxia has the potential to induce polarization of immunosuppressive M2-phenotype TAMs towards tumoricidal M1-phenotype TAMs. The emergence of therapeutic interventions capable of inducing a transition from M2 to M1-phenotype in TAMs has been extensively reported, establishing it as a novel strategy for cancer immunotherapy.[52] The impact of US treatment on the polarization of TAMs was investigated. Tumors were collected 7 days after treatment to prepare cell suspensions for FCM analysis, aiming to determine the composition of distinct TAM phenotypes. The proportion of M1-TAMs in the US-treated group (37.87 ± 1.21%) was significantly higher compared to the control group (23.77 ± 0.90%), aligning with the reduced tumor hypoxia (Figure 3D and E). To further assess the polarization of TAMs, we quantified the secretion levels of two characteristic cytokines (IL-10 and IL-12) produced by M1/M2-TAMs in the serum using ELISA kits. US irradiation was found to significantly enhance the secretion of IL-12, while concurrently reducing the secretion of IL-10, in accordance with FCM results (Figure 3F). The findings suggest that US irradiation holds the potential for alleviating tumor hypoxia and promoting M2-TAM polarization.

Enhanced Anti-Tumor Efficacy of PLD and Anti-PD-L1 with US Irradiation

To investigate the impact of US irradiation on the therapeutic efficacy of PLD and anti-PD-L1, we categorized the unilateral tumor-bearing mice into 8 groups based on the treatment protocols: A: Control, B: US, C: PLD, D: anti-PD-L1, E: PLD + US, F: anti-PD-L1 + US, G: PLD + anti-PD-L1, and H: PLD + anti-PD-L1 + US. The mice received the designated treatments as specified (Figure 4A). The monitoring of mouse tumor volumes (Figure 4B, C and D) demonstrated that despite the successful inhibition of tumor growth in group G (PLD + anti-PD-L1), where chemotherapy and immunotherapy were combined, there was an observed recurrence of tumors within a short period. The tumor growth of mice in group H, which received a combination therapy comprising chemotherapy, immunotherapy, and US irradiation, demonstrated significant inhibition without any observed recurrence. These findings indicate that the treatment modality employed in group H exhibited a pronounced therapeutic effect. The growth curves of tumor volume in groups B, E, F, and H demonstrated a comparatively slower rate compared to those in groups A, C, D, and G, implying that the therapeutic efficacy of combined treatment with US irradiation surpasses that of drug therapy alone. The survival curve revealed that all mice in the single drug group (group C, D, and G) exhibited a 100% survival rate within the range of 0–24 days, whereas the combined treatment group with US (group E, F, and H) demonstrated a significantly prolonged survival period. Notably, all mice in groups G and H surviving at least 32 days or longer (Figure 4E). To further validate the synergistic therapeutic efficacy, histological analysis including H&E and TUNEL staining was conducted on the tumor samples from each group (Figure 4F). The H&E and TUNEL sections revealed that PLD + anti-PD-L1 + US treatment induced severe cell necrosis/apoptosis, while the other groups only exhibited mild or moderate cell damage. These findings suggest that group H receiving PLD + anti-PD-L1 + US treatment achieved robust anti-tumor efficacy.

Anti-Tumor Immune Response

The PD-L1/PD-1 checkpoint blockade, although a promising approach, faces challenges due to insufficient $CD8^+$ T cell infiltration and an immunosuppressive tumor microenvironment.[12,42,53] Transforming “cold tumors“ with inadequate immune cell infiltration into ”hot tumors” represents a crucial strategy for augmenting the effectiveness of immune checkpoint inhibitors.[54–56] Chemotherapy can induce immunogenic cell death (ICD) and elicit the immune response, rendering it a common adjunct to PD-L1/PD-1 checkpoint blockade immunotherapy in clinical settings.[57,58] The infiltration of $CD8^+$ T cells following the combination of US irradiation, chemotherapy, and immunotherapy was investigated by collecting tumor tissues for FCM analysis 7 days after treatment. The results demonstrated a significantly higher proportion of $CD8^+$ T cell infiltration in the groups E, F and H compared to groups C, D, and G (Figure 5A and B). The proportion of $CD8^+$ T cell in group H was approximately 2.6-fold higher compared to the control group (group A). The number of $CD8^+$ T cells in group C after chemotherapy-only was significantly increased

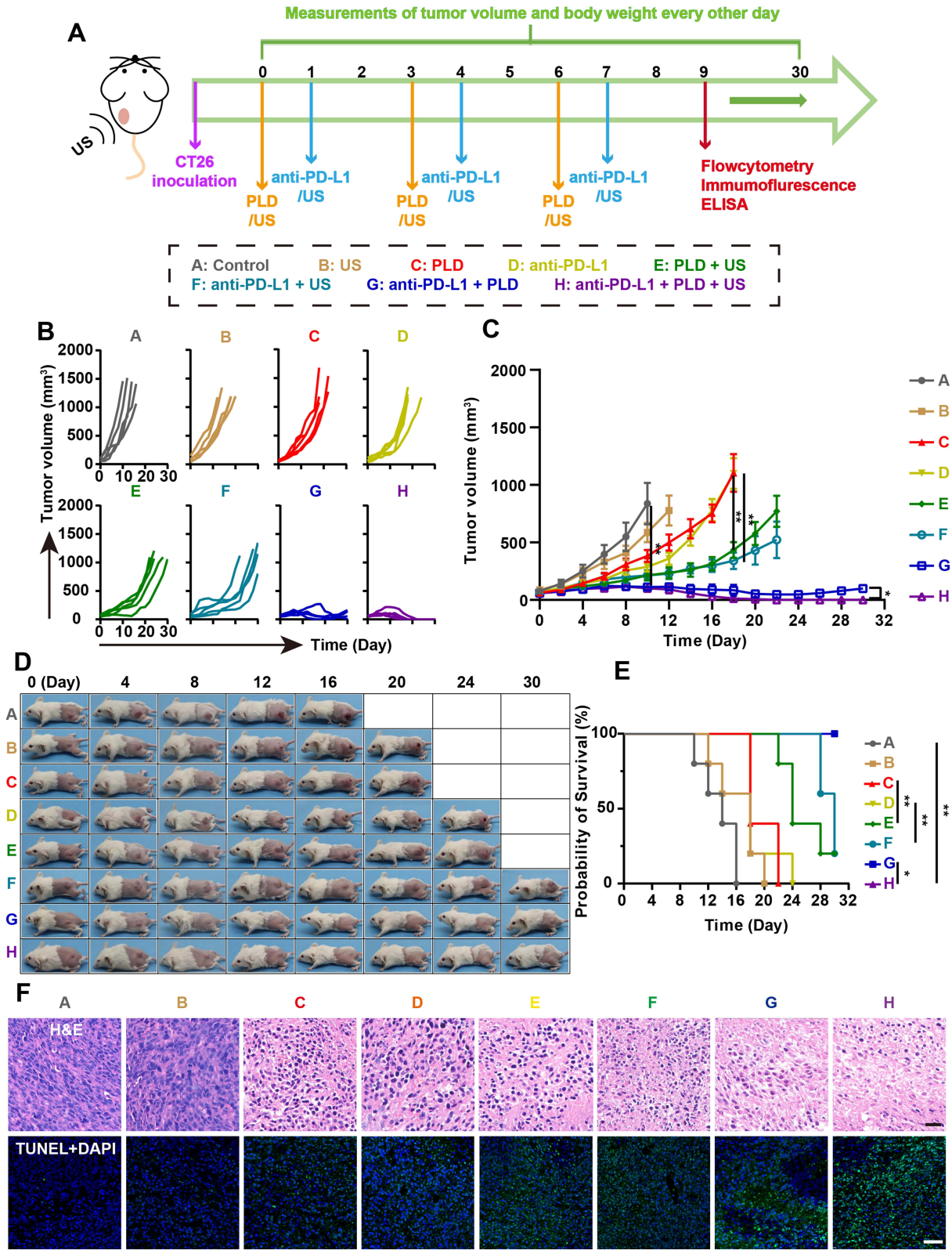

Figure 4 Evaluation of in vivo anti-tumor efficacy. (**A**) Schematic diagram of the treatment process. (**B**) Individual tumor growth curves of CT26 tumor bearing-mice after different treatments (n = 5). (**C**) The average tumor growth curve of CT26 tumor-bearing mice after different treatments (n = 5). (**D**) Representative pictures of tumor growth in CT26 tumor bearing-mice after different treatments. (**E**) Survival analysis of CT26 tumor-bearing mice after different treatments (n = 5). (**F**) H&E and TUNEL staining of tumor slices after various treatments (scale bars = 25 μm). Statistical significances were calculated via Student's *t* test, *p<0.05, **p<0.01.

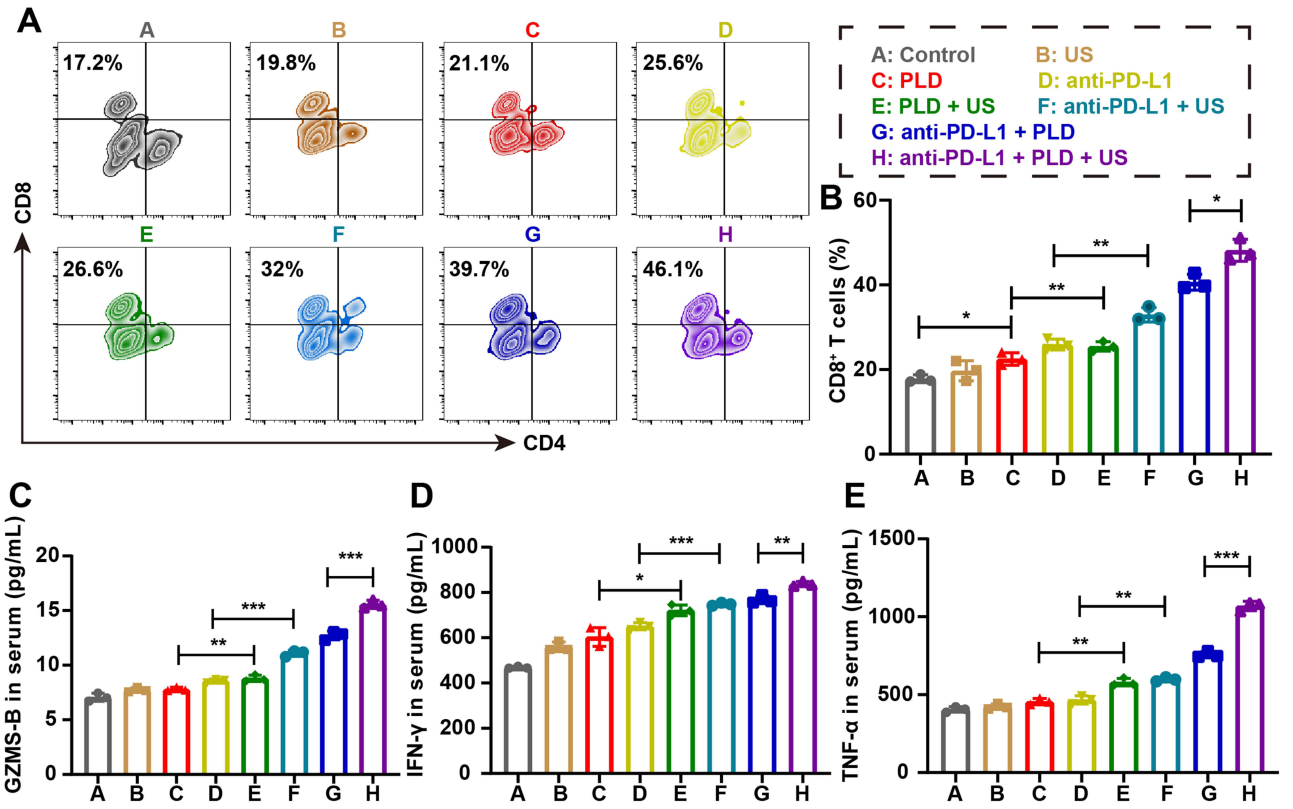

Figure 5 Anti-tumor immune responses after different treatments. (**A-B**) Representative FCM images and quantitative analysis of $CD8^+$ T cells in tumor tissues after different treatments (n = 3). (**C-E**) Cytokine levels of GZMS-B, IFN-γ and TNF-α in serum post various treatments (n = 3). Statistical significances were calculated via Student's *t* test, *p<0.05, **p<0.01, ***p<0.001.

compared to the control group, which can be attributed to the immune response triggered by ICD. To further elucidate the immune response, three cytokines, namely GZMS-B, IFN-γ, and TNF-α, were tested using ELISA kits. Consistent with the results of FCM, the serum levels of these cytokines in US-exposed groups (E, F, H) were significantly higher than in groups C, D, and G (Figure 5C, D and E). Collectively, the therapeutic benefits of US collectively encompass: (1) Enhanced efficiency of drug delivery attributed to the thermal effects induced by US. (2) Alleviation of hypoxia and enhancements in TAMs polarization. (3) Improved infiltration of $CD8^+$ T cells.

The non-invasive and deep penetration capabilities of US have solidified its status as a pervasive modality in clinical applications. The preclinical efficacy of hyperthermia makes the thermal effect of US a feasible approach for tumor therapy. The use of PLD and anti-PD-L1, while commonly used in clinical settings, faces challenges due to aberrant tumor architecture. The integration of these drugs with the US presents a promising therapeutic strategy for overcoming clinical barriers, potentially revolutionizing clinical outcomes and addressing issues related to low drug efficacy and response rates.

Conclusion

In this study, it was found that ultrasonic thermal effect can effectively dilate the blood vessels inside the tumor. When US is administrated at 0.8 W/cm^2 for a duration of 10 min, it significantly enhances the saturation of oxygenated hemoglobin within the tumor, effectively improving the hypoxic microenvironment and further inducing the polarization of TAMs from an M1 to an M2 phenotype. The findings of our study further support the notion that ultrasonic thermal effect-induced tumor vasodilation enhances the intratumoral penetration and infiltration of therapeutic drugs and immune cells, playing a crucial role in improving the effectiveness of chemotherapy and immunotherapy. As a result of US-induced vasodilation, the influx of PLD into the tumor increased by approximately 2.51-fold, while anti-PD-L1 levels rose by approximately 1.44 times. Concurrently, the accumulation of $CD8^+$ T cells in the tumor, coupled with reduced

hypoxia, augmented the anti-PD-L1 response and intratumoral immune response. These synergistic effects led to the effective inhibition of tumor growth, demonstrating the potential of US as a complementary treatment in cancer therapy. The use of US in clinical practice, either as a standalone treatment or in combination with chemotherapy, is considered a safe and non-toxic modality for clinical diagnosis and therapy. PLD and anti-PDL1 are well-established agents in the fields of chemotherapy and immunotherapy respectively, providing a solid foundation for our research to be translated into clinical applications.

Abbreviations

US, ultrasound; ELISA, enzyme-linked immunosorbent assay; PLD, pegylated liposomal doxorubicin; NO, nitric oxide; DOX, doxorubicin; DAPI, 2-(4-amidinophenyl)-6-indolecarbamidinedihydrochloride; anti-PD-L1, PD-L1 antibody; FCM, flow cytometry; TAMs, tumor-associated macrophages; HIFU, high-intensity focused US; CCK-8, cell counting kit-8; Cy5.5, cyanine 5.5 NHS ester; IL, interleukin; TNF-α, tumor necrosis factor-α; IFN-γ, interferon-γ; GZMS-B, granzyme B; eNOs, endothelial nitric oxide synthase; PGI_2, prostaglandin I_2; PGF_2, prostaglandin F_2; C5a, complement fragment 5a; LTC4, leukotriene C4; CFSE, 5.6-carboxyfluorescein diacetate succinimidyl ester; EB, Evans blue; PBS, phosphate-buffered solution; H&E, hematoxylin and eosin; MVD, mean vessel diameter; PA, photoacoustic; HIF-1α, hypoxia-inducible factor 1 alpha; TUNEL, terminal deoxynucleotidyl transferase-mediated dUTP-biotin nick end labeling.

Acknowledgments

This research was supported by the National Natural Science Foundation of China (82202175 and 82171949), Postdoctoral Fellowship Program of CPSF (GZC20233358), China Postdoctoral Science Foundation (2023MD744164), Natural Science Foundation of Chongqing (CSTB2022NSCQ-MSX0093), and Postdoctoral Special Funding Program of Chongqing (2023CQBSHTB3087).

Disclosure

The authors report no conflicts of interest in this work.

References

1. Yu B, Choi B, Li W, Kim DH. Magnetic field boosted ferroptosis-like cell death and responsive MRI using hybrid vesicles for cancer immunotherapy. *Nat Commun*. 2020;11(1):3637. doi:10.1038/s41467-020-17380-5
2. Kok HP, Cressman ENK, Ceelen W, et al. Heating technology for malignant tumors: a review. *Int J Hyperthermia*. 2020;37(1):711–741. doi:10.1080/02656736.2020.1779357
3. Xie J, El Rami F, Zhou K, et al. Multiparameter longitudinal imaging of immune cell activity in chimeric antigen receptor T cell and checkpoint blockade therapies. *ACS Cent Sci*. 2022;8(5):590–602. doi:10.1021/acscentsci.2c00142
4. Cheng X, Shen J, Xu J, et al. In vivo clinical molecular imaging of T cell activity. *Trends Immunol*. 2023;44(12):1031–1045. doi:10.1016/j.it.2023.10.002
5. Huang MY, Jiang XM, Wang BL, Sun Y, Lu JJ. Combination therapy with PD-1/PD-L1 blockade in non-small cell lung cancer: strategies and mechanisms. *Pharmacol & Ther*. 2021;219:107694. doi:10.1016/j.pharmthera.2020.107694
6. Dammeijer F, van Gulijk M, Mulder EE, et al. The PD-1/PD-L1-checkpoint restrains T cell immunity in tumor-draining lymph nodes. *Cancer Cell*. 2020;38(5):685–700.e688. doi:10.1016/j.ccell.2020.09.001
7. Topalian SL, Hodi FS, Brahmer JR, et al. Safety, activity, and immune correlates of anti-PD-1 antibody in cancer. *N Engl J Med*. 2012;366(26):2443–2454. doi:10.1056/NEJMoa1200690
8. Reda M, Ngamcherdtrakul W, Nelson MA, et al. Development of a nanoparticle-based immunotherapy targeting PD-L1 and PLK1 for lung cancer treatment. *Nat Commun*. 2022;13(1):4261. doi:10.1038/s41467-022-31926-9
9. Gieryng A, Pszczolkowska D, Walentynowicz KA, Rajan WD, Kaminska B. Immune microenvironment of gliomas. *Lab Invest*. 2017;97(5):498–518. doi:10.1038/labinvest.2017.19
10. Zhang L, Zhou C, Zhang S, et al. Chemotherapy reinforces anti-tumor immune response and enhances clinical efficacy of immune checkpoint inhibitors. *Front Oncol*. 2022;12:939249. doi:10.3389/fonc.2022.939249
11. Chauhan VP, Jain RK. Strategies for advancing cancer nanomedicine. *Nat Mater*. 2013;12(11):958–962. doi:10.1038/nmat3792
12. Meng Y, Liu H, Zhu H, et al. RCAd-LTH-shPD-L1, a double-gene recombinant oncolytic adenovirus with enhanced antitumor immunity, increases lymphocyte infiltration and reshapes the tumor microenvironment. *J Immunother Cancer*. 2024;12(1):e007171. doi:10.1136/jitc-2023-007171
13. Martin JD, Seano G, Jain RK. Normalizing function of tumor vessels: progress, opportunities, and challenges. *Annu Rev Physiol*. 2019;81(1):505–534. doi:10.1146/annurev-physiol-020518-114700

14. Kang Y, Kim J, Park J, et al. Tumor vasodilation by N-Heterocyclic carbene-based nitric oxide delivery triggered by high-intensity focused ultrasound and enhanced drug homing to tumor sites for anti-cancer therapy. *Biomaterials*. 2019;217:119297. doi:10.1016/j.biomaterials.2019.119297
15. Yang S, Sun B, Li J, et al. Neutrophil extracellular traps promote angiogenesis in gastric cancer. *Cell Commun Signal*. 2023;21(1):176. doi:10.1186/s12964-023-01196-z
16. An YF, Pu N, Jia JB, Wang WQ, Liu L. Therapeutic advances targeting tumor angiogenesis in pancreatic cancer: current dilemmas and future directions. *Biochim Biophys Acta Rev Cancer*. 2023;1878(5):188958. doi:10.1016/j.bbcan.2023.188958
17. Chopra H, Verma R, Kaushik S, et al. Cyclodextrin-based arsenal for anti-cancer treatments. *Crit Rev Ther Drug Carrier Syst*. 2023;40(2):1–41. doi:10.1615/CritRevTherDrugCarrierSyst.2022038398
18. Verma R, Kumar K, Bhatt S, et al. Untangling breast cancer: trailing towards nanoformulations-based drug development. *Recent Pat Nanotechnol*. 2023;40(2):1–41. doi:10.1615/CritRevTherDrugCarrierSyst.20220
19. Cao Z, Liu J, Yang X. Deformable nanocarriers for enhanced drug delivery and cancer therapy. *Exploration*. 2024;20230037. doi:10.1002/EXP.20230037
20. Verma R, Kaushik A, Almeer R, et al. Improved pharmacodynamic potential of rosuvastatin by self-nanoemulsifying drug delivery system: an in vitro and in vivo evaluation. *Int J Nanomed*. 2021;16:905–924. doi:10.2147/IJN.S287665
21. Wang F, Fan Y, Liu Y, et al. Oxygen-carrying semiconducting polymer nanoprodrugs induce sono-pyroptosis for deep-tissue tumor treatment. *Exploration*. 2024:20230100. 10.1002/EXP.20230100.
22. Wang WD, Sun ZJ. Evoking pyroptosis with nanomaterials for cancer immunotherapy: current boom and novel outlook. *Nano TransMed*. 2022;1(1):9130001. doi:10.26599/NTM.2022.9130001
23. Lin H, Song Y, Song L, et al. Inhibition of heat shock-induced H3K9ac reduction sensitizes cancer cells to hyperthermia. *Int J Biol Sci*. 2023;19(15):4849–4864. doi:10.7150/ijbs.86384
24. Zhang C, Wu Y, Zhang Q, et al. The impact of ischemic vascular stenosis on LIPU hyperthermia efficacy investigated based on in vivo rabbit limb ischemia model. *Ultrasonics*. 2024;138:107263. doi:10.1016/j.ultras.2024.107263
25. Paulides MM, Dobsicek Trefna H, Curto S, Rodrigues DB. Recent technological advancements in radiofrequency- andmicrowave-mediated hyperthermia for enhancing drug delivery. *Adv Drug Deliv Rev*. 2020;163-164:3–18. doi:10.1016/j.addr.2020.03.004
26. Moradi Kashkooli F, Souri M, Tavakkoli JJ, et al. A spatiotemporal computational model of focused ultrasound heat-induced nano-sized drug delivery system in solid tumors. *Drug Deliv*. 2023;30(1):2219871. doi:10.1080/10717544.2023.2219871
27. Huaqi Y, Bingqi D, Yanhui Z, et al. Hyperthermia inhibits cellular function and induces immunogenic cell death in renal cell carcinoma. *BMC Cancer*. 2023;23(1):972. doi:10.1186/s12885-023-11106-8
28. Kolosnjaj-Tabi J, Marangon I, Nicolas-Boluda A, Silva AKA, Gazeau F. Nanoparticle-based hyperthermia, a local treatment modulating the tumor extracellular matrix. *Pharmacol Res*. 2017;126:123–137. doi:10.1016/j.phrs.2017.07.010
29. Toraya-Brown S, Fiering S. Local tumour hyperthermia as immunotherapy for metastatic cancer. *Int J Hyperthermia*. 2014;30(8):531–539. doi:10.3109/02656736.2014.968640
30. Vaupel P, Piazena H, Notter M, et al. From localized mild hyperthermia to improved tumor oxygenation: physiological mechanisms critically involved in oncologic thermo-radio-immunotherapy. *Cancers*. 2023;15(5):1394. doi:10.3390/cancers15051394
31. Shirvalilou S, Tavangari Z, Parsaei MH, et al. The future opportunities and remaining challenges in the application of nanoparticle-mediated hyperthermia combined with chemo-radiotherapy in cancer. *Wiley Interdiscip Rev Nanomed Nanobiotechnol*. 2023;15(6):e1922. doi:10.1002/wnan.1922
32. Xia H, Zhu J, Men C, et al. Light-initiated aggregation of gold nanoparticles for synergistic chemo-photothermal tumor therapy. *Nanoscale Adv*. 2023;5(11):3053–3062. doi:10.1039/d3na00114h
33. Stephen ZR, Zhang MA-O. Recent progress in the synergistic combination of nanoparticle-mediated hyperthermia and immunotherapy for treatment of cancer. *Adv Healthc Mater*. 2021;10(2):e2001415. doi:10.1002/adhm.202001415
34. Souri M, Soltani M, Moradi Kashkooli F, et al. Towards principled design of cancer nanomedicine to accelerate clinical translation. *Mater Today Bio*. 2022;13:100208. doi:10.1016/j.mtbio.2022.100208
35. Xu S, Zhang G, Zhang J, et al. Advances in brain tumor therapy based on the magnetic nanoparticles. *Int J Nanomed*. 2023;18:7803–7823. doi:10.2147/IJN.S444319
36. Karmacharya MB, Sultan LR, Hunt SJ, et al. Hydralazine augmented ultrasound hyperthermia for the treatment of hepatocellular carcinoma. *Sci Rep*. 2021;11(1):15553. doi:10.1038/s41598-021-94323-0
37. Song CW, Park H, Griffin RJ. Improvement of tumor oxygenation by mild hyperthermia. *Radiat Res*. 2001;155(4):515–528. doi:10.1667/0033-7587
38. Wang X, Zhang H, Chen X, et al. Overcoming tumor microenvironment obstacles: current approaches for boosting nanodrug delivery. *Acta Biomater*. 2023;166:42–68. doi:10.1016/j.actbio.2023.05.043
39. Liu Y, Zhou J, Li Q, et al. Tumor microenvironment remodeling-based penetration strategies to amplify nanodrug accessibility to tumor parenchyma. *Adv Drug Deliv Rev*. 2021;172:80–103. doi:10.1016/j.addr.2021.02.019
40. Jiang Z, Liu Y, Shi R, et al. Versatile polymer-initiating biomineralization for tumor blockade therapy. *Adv Mater*. 2022;34(19):e2110094. doi:10.1002/adma.202110094
41. Sheybani ND, Price RJ. Perspectives on recent progress in focused ultrasound immunotherapy. *Theranostics*. 2019;9(25):7749–7758. doi:10.7150/thno.37131
42. Huang L, Li Y, Du Y, et al. Mild photothermal therapy potentiates anti-PD-L1 treatment for immunologically cold tumors via an all-in-one and all-in-control strategy. *Nat Commun*. 2019;10(1):4871. doi:10.1038/s41467-019-12771-9
43. Kao TW, Bai GH, Wang TL, et al. Novel cancer treatment paradigm targeting hypoxia-induced factor in conjunction with current therapies to overcome resistance. *J Exp Clin Cancer Res*. 2023;42(1):171. doi:10.1186/s13046-023-02724-y
44. Gao S, Liu M, Liu D, et al. Biomimetic biomineralization nanoplatform-mediated differentiation therapy and phototherapy for cancer stem cell inhibition and antitumor immunity activation. *Asian J Pharm Sci*. 2023;18(5):100851. doi:10.1016/j.ajps.2023.100851
45. Huang J, Leng X, Jiang T, et al. Oxygen-carrying nanoplatform to reprogram tumor immunosuppressive microenvironment and enhance photothermal-immunotherapy. *Mater Today Bio*. 2023;19:100555. doi:10.1016/j.mtbio.2023.100555

46. Zhang L, Wang D, Yang K, et al. Mitochondria-targeted artificial "Nano-RBCs" for amplified synergistic cancer phototherapy by a single NIR irradiation. *Adv Sci*. 2018;5(8):1800049. doi:10.1002/advs.201800049
47. Mortezaee K, Majidpoor J, Kharazinejad E. The impact of hypoxia on tumor-mediated bypassing anti-PD-(L)1 therapy. *Biomed Pharmacother*. 2023;162:114646. doi:10.1016/j.biopha.2023.114646
48. Missiaen R, Lesner NP, Simon MC. HIF: a master regulator of nutrient availability and metabolic cross-talk in the tumor microenvironment. *EMBO J*. 2023;42(6):e112067. doi:10.15252/embj.2022112067
49. Tang YY, Wang DC, Wang YQ, Huang AF, Xu WD. Emerging role of hypoxia-inducible factor-1α in inflammatory autoimmune diseases: a comprehensive review. *Front Immunol*. 2022;13:1073971. doi:10.3389/fimmu.2022.1073971
50. Franklin RA, Liao W, Sarkar A, et al. The cellular and molecular origin of tumor-associated macrophages. *Science*. 2014;344(6186):921–925. doi:10.1126/science.1252510
51. Zhan C, Jin Y, Xu X, Shao J, Jin C. Antitumor therapy for breast cancer: focus on tumor-associated macrophages and nanosized drug delivery systems. *Cancer Med*. 2023;12(10):11049–11072. doi:10.1002/cam4.5489
52. Zhang Y, Li Z, Huang Y, Zou B, Xu Y. Amplifying cancer treatment: advances in tumor immunotherapy and nanoparticle-based hyperthermia. *Front Immunol*. 2023;14:1258786. doi:10.3389/fimmu.2023.1258786
53. Pan X, Ni S, Hu K. Nanomedicines for reversing immunosuppressive microenvironment of hepatocellular carcinoma. *Biomaterials*. 2024;306:122481. doi:10.1016/j.biomaterials.2024.122481
54. Xuan C, Hu R. Chemical biology perspectives on STING agonists as tumor immunotherapy. *ChemMedChem*. 2023;18(23):e202300405. doi:10.1002/cmdc.202300405
55. Yang W, Liu S, Mao M, et al. T-cell infiltration and its regulatory mechanisms in cancers: insights at single-cell resolution. *J Exp Clin Cancer Res*. 2024;43(1):38. doi:10.1186/s13046-024-02960-w
56. Hapuarachi B, Danson S, Wadsley J, Muthana M. Exercise to transform tumours from cold to hot and improve immunotherapy responsiveness. *Front Immunol*. 2023;14:1335256. doi:10.3389/fimmu.2023.1335256
57. Tian Y, Tian H, Li B, Feng C, Dai Y. An ultrasound-triggered STING pathway nanoagonist for enhanced chemotherapy-induced immunogenic cell death. *Small*. 2024. doi:10.1002/smll.202309850
58. Huang X, Ren Q, Yang L, et al. Immunogenic chemotherapy: great potential for improving response rates. *Front Oncol*. 2023;13:1308681. doi:10.3389/fonc.2023.1308681